Analytical Cellular Pathology 25 (2003) 63–75
IOS Press

An original approach for quantification of blood vessels on the whole tumour section

Nga Tran Kim [a,d,*], Nicolas Elie [a,d], Benoît Plancoulaine [b,d], Paulette Herlin [a,d] and Michel Coster [c,d]
[a] *GRECAN, Equipe Universitaire d'Accueil 1772, Centre F. Baclesse, Route de Lion sur Mer, F-14076 Caen, France*
[b] *Département de Mesures Physiques, IUT de Caen, Boulevard du Maréchal Juin, F-14032 Caen, France*
[c] *LERMAT-ISMRA, UPRES-A CNRS 6004, F-14032 Caen, France*
[d] *Pôle Traitement et Analyse d'Images de Basse-Normandie, France*

Received 11 March 2002
Accepted 22 August 2002

Abstract. Relative abundance of tumour angiogenesis has been shown to be of clinical relevance in cancers of various locations such as the ovary. Nevertheless, several problems are encountered when quantifying tumour microvessels: (i) as many other tumour markers, vascularity pattern is often heterogeneous within the tumour mass and even within the same histological section. As a consequence, an adequate acquisition method must be developed for accurate field sampling. (ii) Manual microvessel counting is long, tedious and subject to poor reproducibility. Introduction in routine practice requires a fast, reproducible and reliable automatic image processing.

In this study we present an original procedure combining a slide scanner image acquisition and a fully automatic image analysis sequence. The slide scanner offers the advantage of recording an image of the whole histological section for subsequent automatic blood vessel detection and hot spot area location. Microvessel density and surface fraction were measured for the whole section as well as within hot spots.

Different immunostaining methods were tested in order to optimise the procedure. Moreover, the method proposed was submitted to a quality control procedure, with reference to interactive identification of microvessels at scanner level. This experiment showed that 93 to 97% of blood vessels were detected, according to the staining protocol used. Colour figures can be viewed on http://www.esacp.org/acp/2003/25-2/kim.htm.

Keywords: Angiogenesis, quantification, image analysis, slide scanner

1. Introduction

It is now well established that tumour growth and spread are highly dependent on neo-vascularization [14,32]. A more disputed statement is the prognostic value of tumour angiogenesis. While several studies have demonstrated its predictive significance for clinical outcome in cancers of many locations [1,2,10,12, 17–19,30,39], others failed to find any correlation between tumour vascularity and behaviour [3,4,16,25,27, 28,36]. These discrepancies could be partly explained by differences in microvessel counting methodology, applied to heterogeneous tumours [5,16].

Currently, tumour angiogenesis is assessed by quantifying, at the microscopical level, immunostained blood vessel profiles. More often, tumour microvessels are visually counted at high magnification [3,10, 11,13,17,19,27], but this method is tedious and subject to poor reproducibility. Compared to this procedure, some authors have found the stereological Chalkley point counting method, more reliable [15,23]. Another step towards an objective quantification of tumour angiogenesis was proposed by introducing semi-automatic procedures [6,39]. Nevertheless, these methods still require human intervention for interactive correction or thresholding. Few fully automatic procedures have been recently introduced [7,22,40,41,47].

Whatever the quantification method used, the most critical step remains the identification of the fields to be

*Corresponding author: Tel.: +33 231 45 51 37; Fax: +33 231 45 51 72; E-mail: k.tran@baclesse.fr.

measured. Usually, and according to Weidner's procedure, the quantification is performed in one or several highly vascularized fields (called "hot spots"), previously selected at low magnification by a trained pathologist [43,46]. Other authors have chosen to systematically sample fields over the whole histological section [22] and to average blood vessel density within the most vascularized fields. However, as these authors noted, the reproducibility in systematic tumour sampling is determined by both tumour heterogeneity degree and sampled tumour area, which is defined by the number of sampled fields. The choice of the microscopical magnification also influences the final tumour area analysed, as well as the reliability of the measured parameters [22,34].

Whether the measures obtained within hot spots or all over the section carry the same biological information remains questionable.

In this context, we propose in this paper a fully automatic method for tumour angiogenesis quantification over the whole histological section and inside automatically detected hot spots. The originality of the study is to assess the degree of neovascularization by processing a single numerical image of the whole tumour section, using a photographic slide scanner, provided with a glass slide holder. A quality control was performed in order to assess the robustness of the quantification method and to find the most suitable immunostaining procedure.

2. Material & methods

2.1. Specimens

Formalin-fixed paraffin-embedded samples of 19 human ovarian tumours were cut into 5 μm thick sections and mounted on polylysine coated slides for immunohistochemical staining.

2.2. Immunohistochemistry

Sections were immunolabelled with a polyclonal anti-Von Willebrand Factor antibody (Dako, France), using the Optimax automatic machine (Biogenex) to guarantee staining reproducibility. After deparaffinization and rehydration, slides were heated 30 minutes at 95°C in a citrate buffer (ChemMate^{TM}, Dako) for antigen retrieval. Following incubations were performed at room temperature. Endogenous peroxidase activity was inhibited by incubating sections for 20 minutes in 0.3% H_2O_2. A buffered casein solution (Power Block^{TM}, Biogenex Menarrini, France) was then used to block unspecific binding sites (for 10 minutes). After incubation with the rabbit anti-Von Willebrand Factor antibody (primary antibody, Ab1), 13 and 12 slides were respectively treated by a classical biotin–streptavidin peroxidase technique (series 1) or submitted to signal amplification (series 2) (En Vision^{TM} kit, Dako). Briefly, for classical procedure, after Ab1 incubation (dilution 1 : 50, 1 hour), a biotinylated anti-rabbit antibody (Dako) and then a streptavidin–peroxidase complex (Dako) were applied (dilution 1 : 40, 30 minutes for each reagent). For signal amplification, slides were incubated with peroxidase labelled polymer, conjugated to goat anti-rabbit immunoglobulins for 30 minutes. Staining was completed by incubation, either with diamino-benzidine (DAB) for 10 minutes (series 2a), which stains vessels brown, or with amino-ethylcarbazole (AEC) for 15 minutes (series 2b), which highlights them in red (6 samples for each chromogen, on 2 consecutive sections). Light counterstaining was performed during 10 seconds with Gill's haematoxylin [20] for all specimens.

2.3. Image acquisition

Images of the whole immunostained sections were captured using a 2700 dpi (1 pixel $= 9.4 \times 9.4$ μm) slide scanner (SprintScan ss35Plus, Polaroid, France) provided with a special medical slide holder (PathScan Enabler^{TM}, Meyer Instruments, Inc., USA) and connected to a personal computer (Pentium III, 450 MHz, 128 Mo). Large images (up to 30 megabytes, for sections up to 8 cm^2) were stored as *bitmap* files. These large images of the whole tumour tissue section were directly processed for automatic vessel detection.

2.4. Image processing

Image processing was performed by chaining operators of an image analysis toolbox Aphelion software, v. 3.0 (Adcis, France) implemented on a personal computer and running under Windows operating system.

The procedure can be divided into 5 steps: background correction, tissue detection and necrosis elimination, immunostained structure detection, hot spot identification and location, and measures (Figs 1, 4, Table 1).

Before any analysis, the user can discard normal tissue surrounding the tumour, by drawing regions of interest.

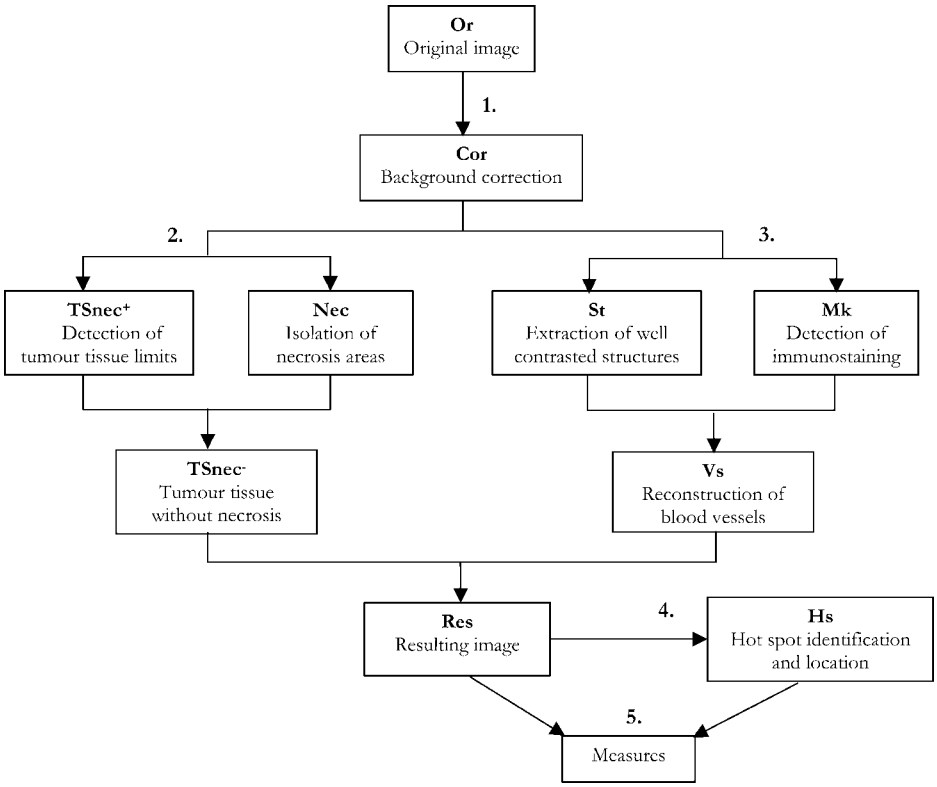

Fig. 1. Strategy for automatic microvessel isolation. The procedure was divided into 5 steps: background correction (1), detection of tumour tissue limits (2), isolation of vessel (3), identification and location of hot spots (4) and measures (5).

Table 1

Measures obtained by the automatic procedure (case presented in Fig. 3). All microvessel profile density (MVD) were expressed as number per mm^2 of tumour tissue. All surface proportions were given as a percentage

Parameters	
Mean microvessel profile density, MVD	40
Mean microvessel surface proportion, MSP	4.5
Mean MVD within hot spot	144
Max MVD within hot spot	387
Mean MSP within hot spot	19
Max MSP within hot spot	30
Surface fraction of hot spots	17

2.4.1. Background correction

The medical slide holder used for scanner acquisition is provided with a 25% transmission filter, which generates a light blue background over the whole image. In order to restore true colours, a correction was applied by selecting a small area, outside the tissue, and setting its grey values to the maximum (255) in the 3 colour channels (Red, Green, and Blue). The 3 RGB values of each pixel of the image were then computed with reference to these new background values.

2.4.2. Tissue detection and necrosis elimination

A fixed threshold, set on the green component of the original image, allowed the detection of the histological section limits ($TSnec^+$). Tumour tissue can contain necrotic areas and mucus which might be deeply stained by chromogens and could appear as large red or brown fields. They were easily removed by thresholding an "excess blue image", a grey scale image generated from the linear combination of the 3 components RGB [50] and computed as follows:

$$f(\mathrm{ExcB}) = 2f(\mathrm{B}) - f(\mathrm{R}) - f(\mathrm{G}).$$

A mathematical morphology closing by reconstruction was set on this grey scale ExcB image. This operator combines a dilatation (square element of size 10) with a geodesic reconstruction (in a 4-connectivity mode[1]). It is used in the same situations as the standard morphological closing, but has the advantage of

[1] In a 4-connectivity mode, only pixels located in the north, south, east and west of a given pixel are considered as neighbour. In a square grid like the one used in this study, these pixels are the closest to the central one.

preserving shape contours. Thereafter, a threshold was set (minimum grey value; 25) and an opening by reconstruction of size 3 was applied on the resulting binary image, to specifically remove small structures, while preserving these large areas. A logical difference between the last image (Nec) and the image of tumour tissue section allowed necrosis elimination ($TSnec^{-}$).

2.4.3. Immunostained structure detection

Detection of highlighted vessels was performed on 2 different images: the first corresponding to the blue channel and the second image (TC) to the following combination:

$$f(\mathrm{TC}) = f(\mathrm{B}) - 0.5f(\mathrm{G}).$$

Firstly, a black top hat transform (difference between closed image and initial image) [35] was applied on the blue image and a fixed threshold (8; 25) was set in order to isolate well-contrasted structures. Structures with holes were filled (hole-fill operator, 4-connectivity mode) and elements cut by the image border were removed (border kill operator, 4-connectivity mode) (St).

Secondly, the brown or red staining deposits were detected by automatically thresholding the TC image (entropy threshold according to Kapur et al. [29]) (Mk).

Objects isolated in this last step (Mk) were used as markers for reconstruction of contrasted structures already characterised (St) (4-connectivity mode). Vessels were reconstructed (Vs) and most false-positive structures were removed using this method (background and unspecific stain deposits). Only elements included in the tissue section were kept by a logical operation (logical AND) between $TSnec^{-}$ and Vs (Res).

2.4.4. Hot spot location

Finally, since the whole histological section was analysed, hot spot areas were identified. For this purpose, neighbouring microvessels were aggregated by closing (square element of size 10) which generates regions of various sizes, according to the number of microvessels joined; small areas ($\leqslant 900\ \mu m^2$) were removed using a 10-size reconstruction by opening (8-connectivity).

2.4.5. Measures

For each image, mean microvessel profile numerical density (MVD, number per surface unit of tumour tissue) and mean microvessel surface proportions (MSP) were determined. Mean and maximum values of MVD and MSP inside identified hot spots were also computed. Finally, the area fraction of hot spots was estimated.

2.5. Quality control procedure

Automatic image processing results in the detection of positive structures (P) as well as false-positive objects (FP). Their respective percentages (%P, %FP) and the percentage of well-detected vessels (%VD) were determined with reference to an interactive identification of vessels.

For this purpose, PaintShop Pro7 (Jasc Software) tools were used for drawing and Aphelion software for computation. Firstly, all vessel profiles observed on the histological section were pointed out, generating a vessel-mask (Vm), caught from the initial image overlay (Fig. 2). The number of dots pointed out on this mask was computed and kept as a reference (nVm).

As mentioned above, the resulting binary image (Res) of the automatic procedure contained well-detected vessels as well as false-positive structures. In order to estimate the proportion of each of them, Res was superimposing on the initial image. By transparency, well-detected vessels could be distinguished from false-positive structures: each structure identified by the observer as a microvessel was interactively pointed out, generating a binary mask called VDm. Structures of Res were then reconstructed from dot markers of VDm. This generated an image of vessels, correctly recognised by the automatic procedures (VD). Image of false-positive structures (FP) was obtained by a logical difference between Res and VD. Interactive pointing was performed in triplicate for each mask (Vm and VDm).

The number of structures present in Res, VD and FP were computed (respectively nRes, nVD and nFP) and the percentage of automatically detected vessel (%VD), positive (%P) and false-positive (%FP) rates were respectively defined as follows:

$$\%\mathrm{VD} = (\mathrm{nVD}/\mathrm{nVm}) \times 100,$$

$$\%\mathrm{P} = (\mathrm{nVD}/\mathrm{nRes}) \times 100,$$

$$\%\mathrm{FP} = 100 - \%\mathrm{P}.$$

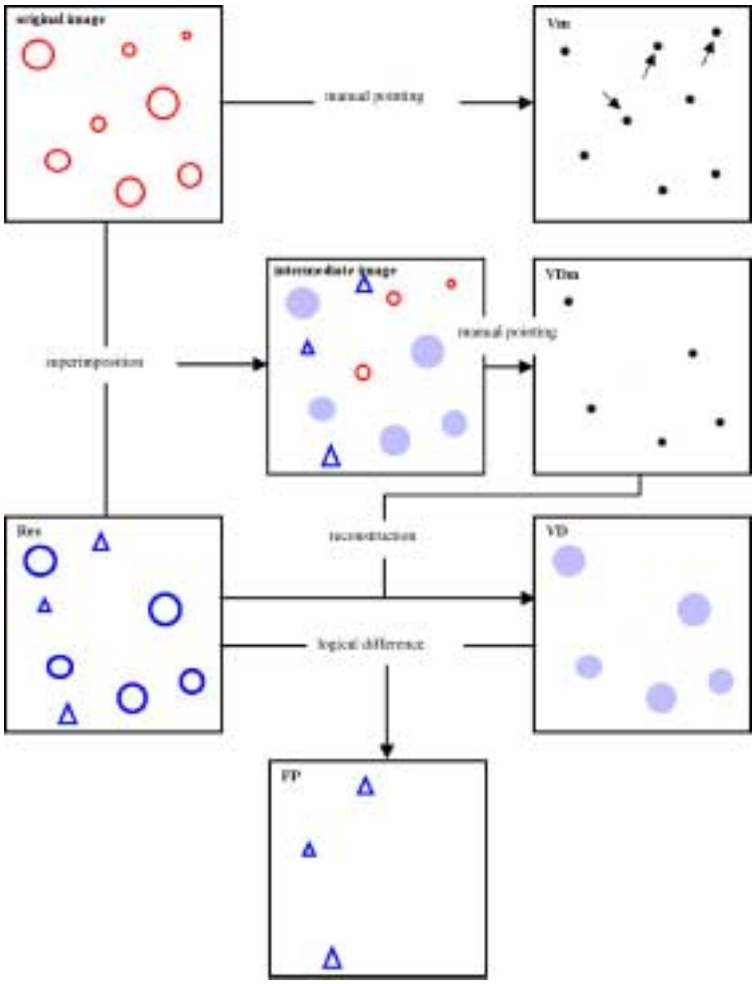

Fig. 2. Principle of the quality control procedure. The true colour original image contains structures of interest of different sizes (circles); a manual pointing of these objects gave the reference mask (Vm). The automatic procedure (binary image Res) detected some of them (circles), and isolated false-positive structures (triangles). The intermediate image shows well-detected objects (full circles), not detected objects (empty circles) and false-positive structures (triangles). A manual pointing of only well-detected objects gave a mask of these structures (VDm). From this mask, structures of Res were reconstructed, given rise to a binary image of these well-detected objects (VD). A logical difference between Res and VD resulted in a binary image of false-positive structures (FP). Object number within Res, VD and FP were computed and percentages of well-detected and false-positive structures were calculated as described in methods. This figure can be viewed on http://www.esacp.org/acp/2003/25-2/kim.htm.

One can notice that:

$$\mathrm{nRes} = \mathrm{nVD} + \mathrm{nFP}.$$

Surface fraction of both correctly detected vessels ($\mathrm{MSP_{VD}}$) and false-positive structures ($\mathrm{SP_{FP}}$) were also determined. The relative surface proportion (rSP) of false-positive *vs.* correctly detected vessels was defined as follows:

$$\mathrm{rSP} = (\mathrm{SP_{FP}}/\mathrm{MSP_{VD}}) \times 100.$$

Furthermore, a quality factor was computed [9] as follows:

$$Qt = \big(\%\mathrm{VD} \times (100 - \%\mathrm{FP})\big)/100$$

the higher the Qt, the better the result ($Qt_{\max} = 100$).

This control procedure was used to evaluate the quality of automatic microvessel detection and to compare results obtained by the various staining procedures tested:

(i) Immunostaining by classical (biotin–streptavidin peroxidase) and amplified (EnVison kit) method (DAB as chromogen for both staining methods),

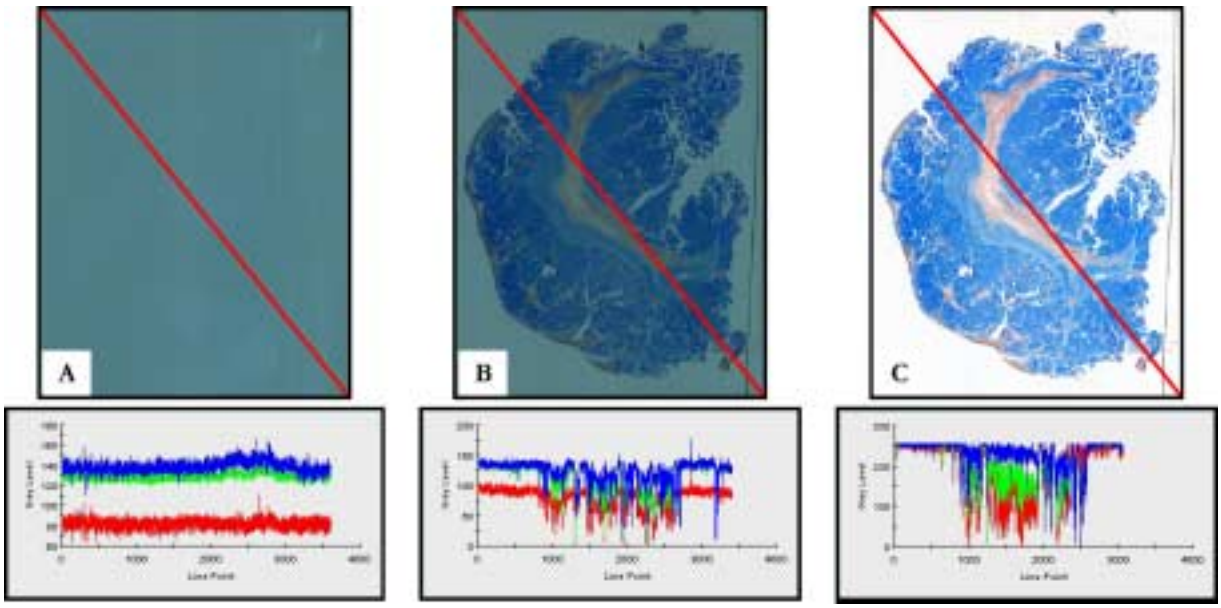

Fig. 3. Image uniformity. Images of the slide holder filter (A), of a whole histological section before (B) and after background correction (C), and their corresponding profile along the red line. This figure can be viewed on http://www.esacp.org/acp/2003/25-2/kim.htm.

(ii) Highlighting blood vessels in brown (DAB as a chromogen) and in red (AEC as a chromogen).

3. Results

3.1. Automatic microvessel detection from scanner images

The filter of the medical slide holder provides a uniform blue background over the whole image. Profiles obtained in the three channels along a diagonal line, drawn across the image show that this background is at the same level all over the image; it can then be easily removed by a fixed threshold (Fig. 3).

Figure 4 shows an example of automatic microvessel extraction from a scanner image of a whole histologic section. It takes nearly 15 minutes to process such a 30-Mb image. An interactive delineation of the tumour was first set for removing normal tissue (Fig. 4A). All the following steps were automatically done: tumour tissue contour detection, necrotic areas and mucus removing, vessel detection and hot spot identification.

Microvessel profiles extracted in this example represent 4.5% of the tumour section area; mean microvessel profile density (MVD) inside the entire tumour section was of 40 vessel profiles/mm^2 (Table 1).

Many hot spots were located and visualised on the whole image. These highly vascularized areas represent 17% of the tumour section. The mean and the maximum MVD values inside these hot spots were respectively of 144 and 387 vessel profiles/mm^2. The mean surface proportion of these microvessel profiles (MSP) inside the hot spots was 19% and its maximum was 30%.

3.2. Quality control of the automatic detection

Compared to interactive vessel pointing, most vessel profiles were detected (mean %VD: 97%) after classical immunolabelling and DAB staining, with a mean %FP of 22% (range 14–37%) (Fig. 5). Images with a %FP beyond 30% (T4 and T7) correspond to unsatisfactory stained sections (background and reagent deposits). The mean quality factor Qt obtained reached 75% for the 13 cases studied (range 63–83%).

3.3. Method robustness with regard to the staining procedure used

Results of microvessel automatic detection on images of tumour section, immunostained by classical and amplified method (EnVison kit) are given in Fig. 6 (DAB as a chromogen for both staining method). For an equivalent mean %VD (97%), %FP was higher (mean %FP: 30%) and reached 51% in

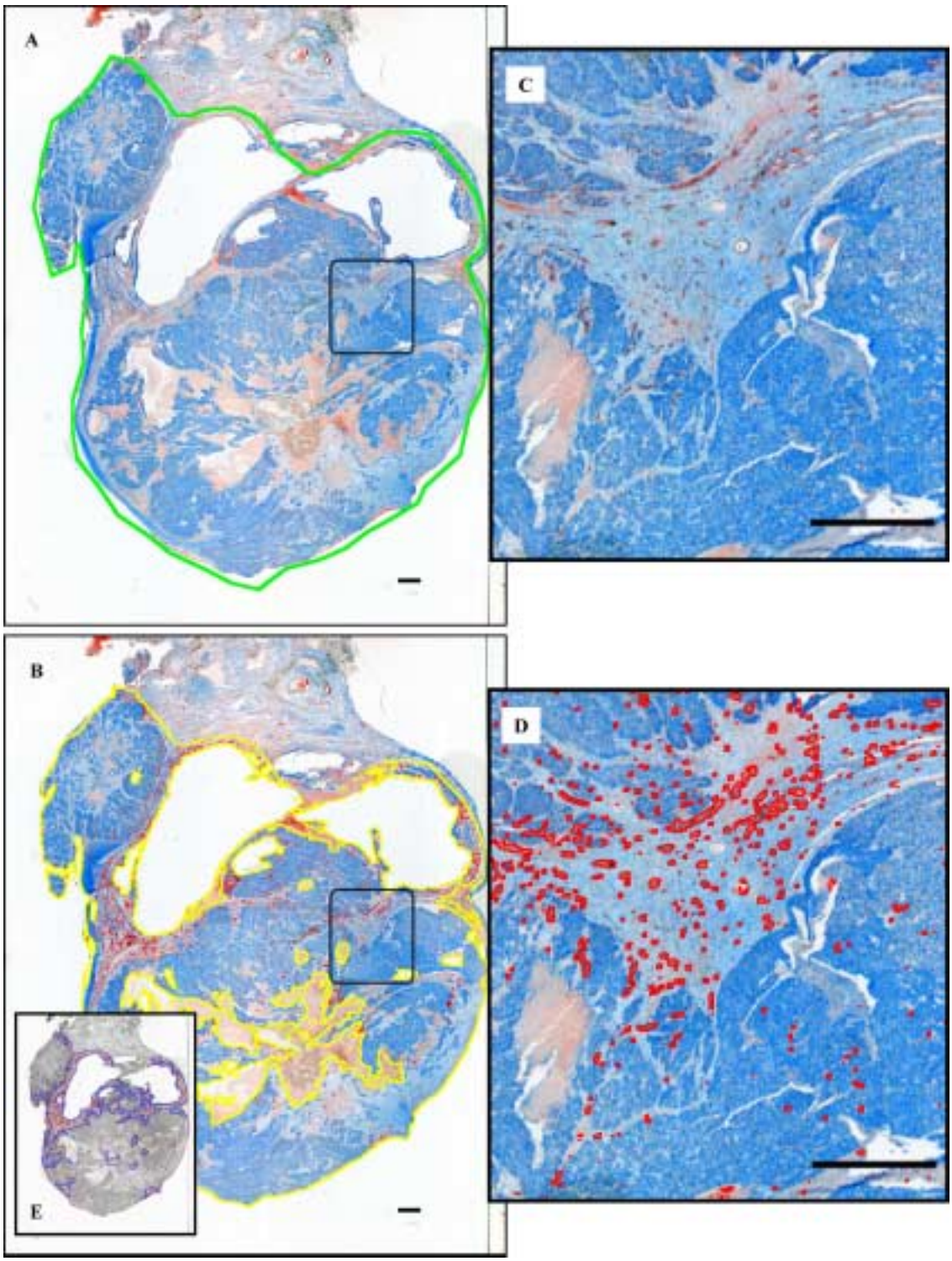

Fig. 4. Example of automatic microvessel isolation on scanner image. (A) Image of the whole histological section. The normal tissue was eliminated from analysis by a manual delineation (green line). (B) Tumour tissue edges were automatically detected, necrotic and mucus deposits were eliminated (yellow lines). Blood vessels were isolated (red underlining). (C and D) Detail of the tumour tissue before (C) and after (D) blood vessel detection. (E) Hot spot identification (blue line). Bars, 1 mm. This figure can be viewed on http://www.esacp.org/acp/2003/25-2/kim.htm.

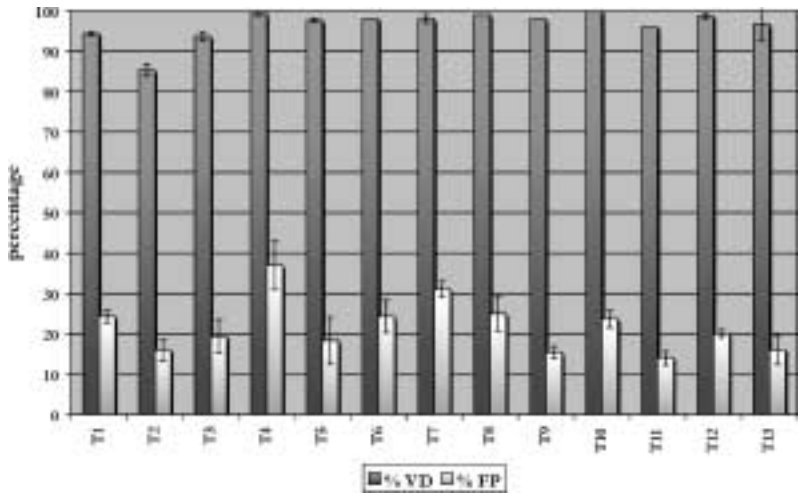

Fig. 5. Percentages of well-detected vessels (%VD) and of false-positive structures (%FP) on scanner image, by reference with interactive identification. Vessels were classically immunostained using DAB as chromogen (series 1).

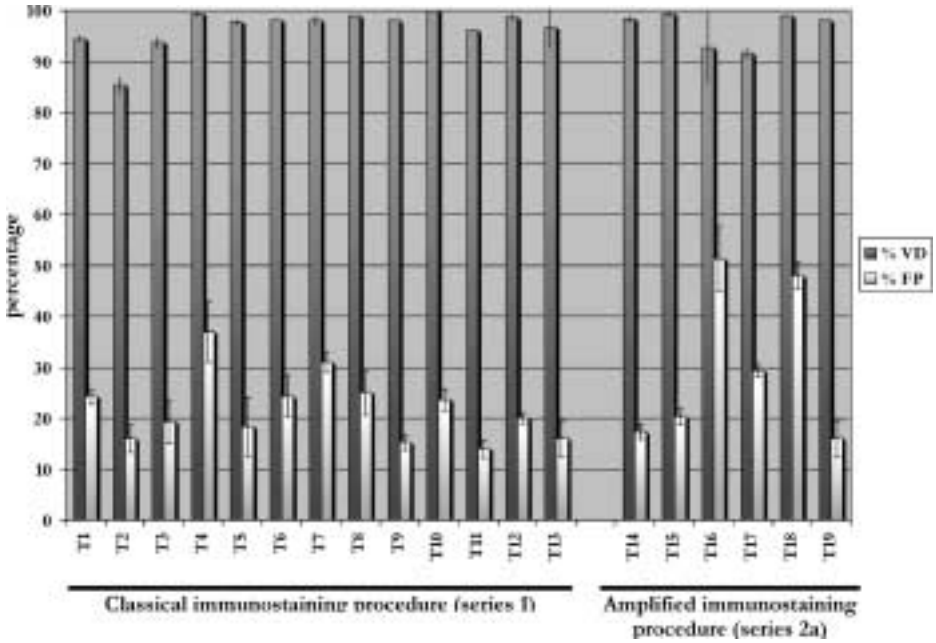

Fig. 6. Comparison of results obtained after classical and enhanced immunostaining procedure. Well detected vessel (%VD) and false-positive (%FP) rates were determined for each labelling method used. DAB was used as chromogen for both sets.

one case (T16) when amplifying the signal. This was confirmed by a lower mean Qt of 64% (range 45–82%).

Comparing results obtained on images of two consecutive sections of the same tumour, immunostained by DAB or AEC, showed (Fig. 7) that mean %VD was lower when using AEC (93%) than DAB (97%) but less false-positives were obtained with AEC, since mean %FP was of 26%, against 51% with DAB. This resulted in a better mean Qt with AEC (69%, range 52–85%) than with DAB (64%, range 45–82%).

Furthermore, the analysis of the relative surface proportion of false-positive structures *vs.* detected vessels (rSP) showed that automatic image processing isolated false-positives of relatively small size (mean rMSP $=$ 11.85%, range 6.57–23.19%) when vessels of tumour sections were classically stained with DAB (Fig. 8). In contrast, mean rSP was 21.45%

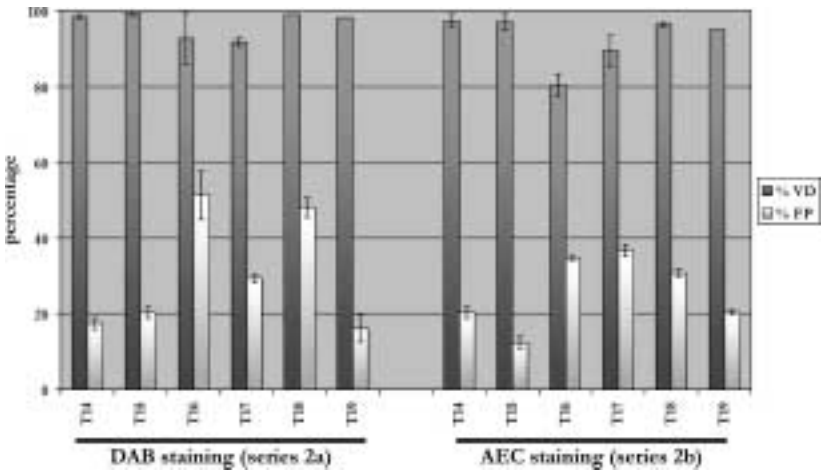

Fig. 7. Comparison of results obtained with DAB and AEC as chromogens. Both chromogens were used with the amplified immunostaining procedure. Well detected vessel (%VD) and false-positive (%FP) rates were determined for each image.

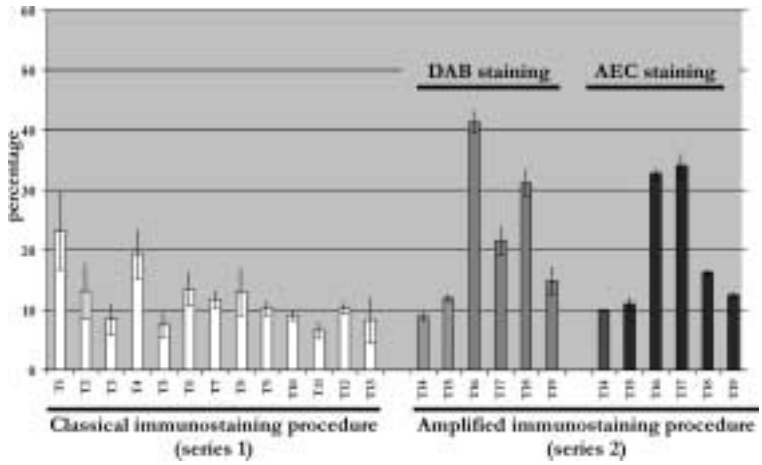

Fig. 8. Comparison of the relative surface proportion of false-positive *vs.* positive structures obtained after classical and enhanced immunostaining procedures. This relative surface proportion (rSP) was defined as a ratio: (surface proportion of false-positives/surface proportion of positives) $\times$ 100. rSP was determined for series 1 and series 2.

(range 8.95–41.31%) and 19.42% respectively (range 9.91–34.06%) when the amplification protocol was used, either with DAB or AEC, showing that larger false-positives were detected.

4. Discussion

Colour figures can be viewed on http://www.esacp.org/acp/2003/25-2/kim.htm. Results presented here underline the advantages of an original image acquisition method, coupled to an automatic image analysis procedure, for angiogenesis quantification on immunostained tumour sections. The slide scanner offers the opportunity of obtaining an image of the whole histological section, which can be processed in one step. The observer can also discard normal tissue from analysis by selecting a region of interest inside this image. Reproducibility in vessel detection and hot spot identification is possible using this strategy. Furthermore, this approach provides a solution to the major problem of tumour tissue heterogeneity. Indeed, discrepancies found in literature can be partly explained by the bias introduced by human intervention in field selection, hot spot identification or vessel counting [7, 46,49], amplified by the well-known problem of biological heterogeneity of tumours (and in particular, intra-tumoural vascular heterogeneity) [5,16].

In such a context, two major points have to be solved: the choice of the parameter to be measured and the measurement method. Concerning the first point, whether the measurement within the most vascularized fields (called "hot spots") is more significant than an average value obtained over the whole section, remains uncertain. Most authors assess tumour angiogenesis by estimating microvessel numerical density (number of profiles per unit area), within hot spots [15, 21,33,46]. In these conditions, it is impossible to distinguish uniformly from focally well-vascularized tumours, whose behaviour may be quite different. Only confrontation or combination of data obtained from the whole tissue and from hot spots could give a reliable answer, considering moreover that the presence of such highly vascularized fields is not always obvious. In this manner, Kato et al. showed that the average of microvessel density, but not the highest value, was an independent prognostic indicator in breast cancer [30,31]. The procedure proposed here has the advantage of providing both values, together with the mean value within all hot spots identified on the section. Furthermore, an estimate of the area fraction of hot spots is given.

As vascular density obtained using such an automatic image analysis method may be biased by imperfect segmentation of microvessels (which can aggregate neighbouring profiles or can split a single one into several unconnected fragments), vascular area fraction is given in addition and should be preferred. One must notice that some authors have already suggested that vascular area fraction should also be considered as an important parameter [15,38,47]. Which of these parameters have the strongest clinical information will be determined by studying large series of patients.

The manner in which the fields to be measured are chosen is a very critical step. To give a mean value over the whole section at microscopical level, it is necessary to acquire all fields or to systematically sample the histological section and take into account the mean value. The first solution is time consuming and needs large image storage capacities. The second method is more attractive, but, as previously mentioned, the reproducibility in systematic tumour sampling is determined by both tumour heterogeneity degree and sampled tumour area, which is defined by the number of sampled fields [22]. Acquisition by a slide scanner solved this sampling problem as the histological section is analysed as a whole from a single image (of at most 30 Mb).

If the quantification must be assessed within hot spots, their identification has to be as objective as possible, to ensure reproducibility of data. For this purpose, several authors proposed to sample and analyse the whole section at microscopical level. Vascular parameters are automatically assessed for each field and hot spots are then identified [7,41]. For example, Van der Laak et al. averaged the three highest values obtained in separate fields over the whole section [41]. However, since these fields can be spread out across the histological section, this could not be considered as a true hot spot. To the best of our knowledge, only a recent study proposed an objective identification of hot spots covering more than one microscopical field [7]. The authors presented an automatic blood vessel detection and mapping over the whole section; afterwards, the authors automatically identified hot spot areas from this map. However, as noted by authors, the "automatically" identified hot spots did not always fit with those identified visually, indicating that interactive selection of hot spots, as usually performed, may be biased. Furthermore, the study in question underlined that results obtained were dependent on the shape of hot spots, defined by the observer. In the same way, the hot spot identification procedure presented in this paper is dependent on the size of the structuring element used, which defines the distance between microvessels to be aggregated. In the present study, hot spot areas were determined by joining microvessels distant from at most 200 μm. This distance was determined considering several data available in the literature: (i) the distance between perfused vessel and hypoxic regions in tumours varied from 50 to 150 μm (mean 100 μm) [24,37,42,45,48]. Beyond this distance from the nearest blood vessel, cells die due to the lack of oxygen and nutrient supply, and undergo necrosis [8,37,48]. So, the maximum inter-vessel distance may be nearly 200 μm. (ii) In invasive breast carcinoma, Belien et al. found a majority of mitotic figures between 0 and 102–268 μm, and a sharp decrease of them beyond a distance of 100 μm from the nearest blood vessel [8]. Then, aggregating vessels separated by a distance lower than or equal to 200 μm is in agreement with previously published data.

Another point to be discussed is the 3D sampling. One must notice that, although removing subjectivity in 2D section sampling, the results obtained here do not take into account 3D-tumour heterogeneity. They were collected from a single slide chosen as "the most representative" of the tumour mass. This "one slide" analysis has some chances to be successfully introduced in

routine practice. Nevertheless, the simplicity, low cost and rapidity of the proposed method allow serial section analysis. 3D sampling could be solved if the investigator applies stereological rules; some equipment, such as the tissue slicer, may be helpful for assessing this manipulation [26].

Once the sampling strategy is chosen, a reproducible quantification procedure has to be used. Only a fully automatic system can ensure this reproducibility. Nevertheless, the quality of such a procedure is highly dependent on specimen preparation (especially on tissue staining) [47], and on the resolution of the acquisition material used.

Concerning the first point, recent papers show that signal amplification with biotinylated tyramine improved vessel staining, with poor background noise [7,22]. The quality control of the presented method showed that the signal amplification used generated noise thus giving rise to false-positive events. Automatic quantification procedures found in literature, allow the user to interactively remove false-positive structures; the method proposed in our paper discards any human intervention, but a percentage of microvessels detected as well as an estimate of false-positive objects were evaluated. In addition, it has been reported that the investigator's experience influences the result obtained [6,44]. A fully automatic system does not require extensive training. Furthermore, to be adapted to clinical routine, a method for biological marker quantification ought to be simple and fast. Fully automatic procedures have been already noted to be faster than semi-automatic or manual ones [7,47]. The procedure we propose takes only 15 minutes to analyse a section of approximately 5 cm^2, as opposed to previously published time consuming methods [7].

Concerning the resolution of the acquisition system, it must be high enough to ensure catching all structures of interest. The quality control performed in the present study showed that most microvessels, interactively identified, were detected (93 to 97%, according to a staining with AEC or DAB). However, it does not guarantee that all microvessels present on the tumour section were detectable by the human eye at scanner level. To answer this question, the procedure developed should be more extensively compared to classical microscopic image processing in order to appraise the possibly lost vessels (work in progress). Moreover, the prognostic value of the vascular parameters provided at scanner level is now being evaluated through a multivariate analysis of clinical and biological markers from a large series of ovarian tumours.

Acknowledgements

This work was supported by grants from the "Comités départementaux de la Ligue contre le Cancer de la Manche et du Calvados". Miss Tran is a fellow of the first committee.

The authors would like to thank any person who has contributed to this work and particularly Heather Costil, Yves Denoux, Abderahim Elmoataz and Christian Lebeau.

References

[1] O. Abulafia and D.M. Sherer, Angiogenesis in the uterine cervix, *Int. J. Gynecol. Cancer* **10**(5) (2000), 349–357.

[2] O. Abulafia, W.E. Triest and D.M. Sherer, Angiogenesis in primary and metastatic epithelial ovarian carcinoma, *Am. J. Obstet. Gynecol.* **177**(3) (1997), 541–547.

[3] M.J. Ahn, C.K. Park, J.H. Choi, W.M. Lee, Y.Y. Lee, I.Y. Choi, I.S. Kim, W.S. Lee and M. Ki, Clinical significance of microvessel density in multiple myeloma patients, *J. Korean Med. Sci.* **16**(1) (2001), 45–50.

[4] L.A. Akslen and V.A. Livolsi, Increased angiogenesis in papillary thyroid carcinoma but lack of prognostic importance, *Hum. Pathol.* **31**(4) (2000), 439–442.

[5] K. Axelsson, B.M. Ljung, D.H. Moore, A.D. Thor, K.L. Chew, S.M. Edgerton, H.S. Smith and B.H. Mayall, Tumor angiogenesis as a prognostic assay for invasive ductal breast carcinoma, *J. Natl. Cancer Inst.* **87**(13) (1995), 997–1008.

[6] M. Barbareschi, N. Weidner, G. Gasparini, L. Morelli, S. Forti, C. Eccher, P. Fina, O. Caffo, E. Leornardi, F. Mauri, P. Bevilacqua and P. Dalla Palma, Microvessel density quantification in breast carcinomas, *Appl. Immunohistochem.* **3**(2) (1995), 75–84.

[7] J.A. Belien, S. Somi, J.S. de Jong, P.J. van Diest and J.P. Baak, Fully automated microvessel counting and hot spot selection by image processing of whole tumour sections in invasive breast cancer, *J. Clin. Pathol.* **52**(3) (1999), 184–192.

[8] J.A. Belien, P.J. van Diest and J.P. Baak, Relationships between vascularization and proliferation in invasive breast cancer, *J. Pathol.* **189**(3) (1999), 309–318.

[9] C. Boudry, P. Herlin, B. Plancoulaine, E. Masson, A. Elmoataz, H. Cardot, M. Coster, D. Bloyet and J.L. Chermant, Automatic morphological sieving: comparison between different methods, application to DNA ploidy measurements, *Anal. Cell. Pathol.* **18**(4) (1999), 203–210.

[10] L. Cagini, M. Monacelli, G. Giustozzi, L. Moggi, G. Bellezza, A. Sidoni, E. Bucciarelli, S. Darwish, V. Ludovini, L. Pistola, V. Gregorc and M. Tonato, Biological prognostic factors for early stage completely resected non-small cell lung cancer, *J. Surg. Oncol.* **74**(1) (2000), 53–60.

[11] C. Charpin, B. Devictor, D. Bergeret, L. Andrac, J. Boulat, N. Horschowski, M.N. Lavaut and L. Piana, CD31 quantitative immunocytochemical assays in breast carcinomas. Correlation with current prognostic factors, *Am. J. Clin. Pathol.* **103**(4) (1995), 443–448.

[12] J.G. Edwards, G. Cox, A. Andi, J.L. Jones, R.A. Walker, D.A. Waller and K.J. O'Byrne, Angiogenesis is an independent prognostic factor in malignant mesothelioma, *Br. J. Cancer* **85**(6) (2001), 863–868.

[13] C. Erenoglu, M.L. Akin, H. Uluutku, L. Tezcan, S. Yildirim and A. Batkin, Angiogenesis predicts poor prognosis in gastric carcinoma, *Dig. Surg.* **17**(6) (2000), 581–586.

[14] J. Folkman, What is the evidence that tumors are angiogenesis dependent?, *J. Natl. Cancer Inst.* **82**(1) (1990), 4–6.

[15] S.B. Fox, R.D. Leek, M.P. Weekes, R.M. Whitehouse, K.C. Gatter and A.L. Harris, Quantitation and prognostic value of breast cancer angiogenesis: comparison of microvessel density, Chalkley count, and computer image analysis, *J. Pathol.* **177**(3) (1995), 275–283.

[16] V. Fridman, C. Humblet, K. Bonjean and J. Boniver, Assessment of tumor angiogenesis in invasive breast carcinomas: absence of correlation with prognosis and pathological factors, *Virchows Arch.* **437**(6) (2000), 611–617.

[17] S. Fujioka, K. Yoshida, S. Yanagisawa, M. Kawakami, T. Aoki and Y. Yamazaki, Angiogenesis in pancreatic carcinoma: thymidine phosphorylase expression in stromal cells and intratumoral microvessel density as independent predictors of overall and relapse-free survival, *Cancer* **92**(7) (2001), 1788–1797.

[18] G. Gasparini, Clinical significance of the determination of angiogenesis in human breast cancer: update of the biological background and overview of the Vicenza studies, *Eur. J. Cancer* **32A**(14) (1996), 2485–2493.

[19] A. Giatromanolaki, E. Sivridis, R. Brekken, P.E. Thorpe, P. Anastasiadis, K.C. Gatter, A.L. Harris and M.I. Koukourakis, The angiogenic "vascular endothelial growth factor/flk-1(KDR) receptor" pathway in patients with endometrial carcinoma: prognostic and therapeutic implications, *Cancer* **92**(10) (2001), 2569–2577.

[20] G.M. Gill, J.K. Frost and K.A. Miller, A new formula for a half-oxidilized hematoxylin solution which never overstains nor requires differentiation, *Acta Cytol.* **18**(4) (1974), 300–311.

[21] A.J. Guidi, D.A. Berry, G. Broadwater, M. Perloff, L. Norton, M.P. Barcos and D.F. Hayes, Association of angiogenesis in lymph node metastases with outcome of breast cancer, *J. Natl. Cancer Inst.* **92**(6) (2000), 486–492.

[22] E.J. Hannen, J.A. Der Laak, H.M. Kerstens, V.M. Cuijpers, A.G. Hanselaar, J.J. Manni and P.C. de Wilde, Quantification of tumour vascularity in squamous cell carcinoma of the tongue using CARD amplification, a systematic sampling technique, and true colour image analysis, *Anal. Cell. Pathol.* **22**(4) (2001), 183–192.

[23] S. Hansen, D.A. Grabau, C. Rose, M. Bak and F.B. Sorensen, Angiogenesis in breast cancer: a comparative study of the observer variability of methods for determining microvessel density, *Lab. Invest.* **78**(12) (1998), 1563–1573.

[24] H.K. Haugland, V. Vukovic, M. Pintilie, A.W. Fyles, M. Milosevic, R.P. Hill and D.W. Hedley, Expression of hypoxia-inducible factor-1alpha in cervical carcinomas: correlation with tumor oxygenation, *Int. J. Radiat. Oncol. Biol. Phys.* **53**(4) (2002), 854–861.

[25] C. Herbst, H. Kosmehl, K.J. Stiller, A. Berndt, M. Eiselt, J. Schubert and D. Katenkamp, Evaluation of microvessel density by computerised image analysis in human renal cell carcinoma. Correlation to pT category, nuclear grade, proliferative activity and occurrence of metastasis, *J. Cancer Res. Clin. Oncol.* **124**(3–4) (1998), 141–147.

[26] C.V. Howard and M.G. Reed, *Unbiased Stereology – Three-Dimensional Measurement in Microscopy*, BIOS Scientific Publishers Limited, Oxford, 1998.

[27] G. Juric, N. Zarkovic, M. Nola, M. Tillian and S. Jukic, The value of cell proliferation and angiogenesis in the prognostic assessment of ovarian granulosa cell tumors, *Tumori* **87**(1) (2001), 47–53.

[28] Y.H. Kang, K.S. Kim, Y.K. Yu, S.C. Lim, Y.C. Kim and K.O. Park, The relationship between microvessel count and the expression of vascular endothelial growth factor, p53, and K-ras in non-small cell lung cancer, *J. Korean Med. Sci.* **16**(4) (2001), 417–423.

[29] J.N. Kapur, A.K.C. Sahoo and A. Wong, A new method for grey-level picture thresholding using the entropy of the histogram, *Computer Vision, Graphics, and Image Processing* **29** (1985), 273–285.

[30] T. Kato, S. Kameoka, T. Kimura, N. Soga, Y. Abe, T. Nishikawa and M. Kobayashi, Angiogenesis as a predictor of long-term survival for 377 Japanese patients with breast cancer, *Breast Cancer Res. Treat.* **70**(1) (2001), 65–74.

[31] T. Kato, T. Kimura, N. Ishii, A. Fujii, K. Yamamoto, S. Kameoka, T. Nishikawa and T. Kasajima, The methodology of quantitation of microvessel density and prognostic value of neovascularization associated with long-term survival in Japanese patients with breast cancer, *Breast Cancer Res. Treat.* **53**(1) (1999), 19–31.

[32] R.S. Kerbel, Tumor angiogenesis: past, present and the near future, *Carcinogenesis* **21**(3) (2000), 505–515.

[33] P.D. Kohlberger, A. Obermair, G. Sliutz, H. Heinzl, H. Koelbl, G. Breitenecker, G. Gitsch and C. Kainz, Quantitative immunohistochemistry of factor VIII-related antigen in breast carcinoma: a comparison of computer-assisted image analysis with established counting methods [see comments], *Am. J. Clin. Pathol.* **105**(6) (1996), 705–710.

[34] L. Martin, C. Holcombe, B. Green, S.J. Leinster and J. Winstanley, Is a histological section representative of whole tumour vascularity in breast cancer?, *Br. J. Cancer* **76**(1) (1997), 40–43.

[35] F. Meyer, IIième symposium européen d'analyse d'images en sciences des matériaux, biologie et médecine, Caen, France, 4/7 Oct. 1977, *Pract. Met.* **S8** (1978), 374–380.

[36] B.V. Offersen, P. Pfeiffer, S. Hamilton-Dutoit and J. Overgaard, Patterns of angiogenesis in nonsmall-cell lung carcinoma, *Cancer* **91**(8) (2001), 1500–1509.

[37] P.F. Rijken, H.J. Bernsen, J.P. Peters, R.J. Hodgkiss, J.A. Raleigh and A.J. van der Kogel, Spatial relationship between hypoxia and the (perfused) vascular network in a human glioma xenograft: a quantitative multi-parameter analysis, *Int. J. Radiat. Oncol. Biol. Phys.* **48**(2) (2000), 571–582.

[38] J.F. Simpson, C. Ahn, H. Battifora and J.M. Esteban, Endothelial area as a prognostic indicator for invasive breast carcinoma, *Cancer* **77**(10) (1996), 2077–2085.

[39] W. Tjalma, E. Van Marck, J. Weyler, L. Dirix, A. Van Daele, G. Goovaerts, G. Albertyn and P. van Dam, Quantification and prognostic relevance of angiogenic parameters in invasive cervical cancer [see comments], *Br. J. Cancer* **78**(2) (1998), 170–174.

[40] J.A. Van der Laak, M.M. Pahlplatz, A.G. Hanselaar and P.C. de Wilde, Hue-saturation-density (HSD) model for stain recognition in digital images from transmitted light microscopy, *Cytometry* **39**(4) (2000), 275–284.

[41] J.A. Van der Laak, J.R. Westphal, L.J. Schalkwijk, M.M. Pahlplatz, D.J. Ruiter, R.M. de Waal and P.C. de Wilde, An improved procedure to quantify tumour vascularity using true colour image analysis. Comparison with the manual hot-spot procedure in a human melanoma xenograft model, *J. Pathol.* **184**(2) (1998), 136–143.

[42] B.P. Van der Sanden, P.F. Rijken, A. Heerschap, H.J. Bernsen and A.J. van der Kogel, In vivo (31)P magnetic resonance spectroscopy and morphometric analysis of the perfused vascular architecture of human glioma xenografts in nude mice, *Br. J. Cancer* **75**(10) (1997), 1432–1438.

[43] P.B. Vermeulen, G. Gasparini, S.B. Fox, M. Toi, L. Martin, P. McCulloch, F. Pezzella, G. Viale, N. Weidner, A.L. Harris and L.Y. Dirix, Quantification of angiogenesis in solid human tumours: an international consensus on the methodology and criteria of evaluation, *Eur. J. Cancer* **32A**(14) (1996), 2474–2484.

[44] P.B. Vermeulen, M. Libura, J. Libura, P. J. O'Neill, P. van Dam, E. Van Marck, A.T. Van Oosterom and L.Y. Dirix, Influence of investigator experience and microscopic field size on microvessel density in node-negative breast carcinoma, *Breast Cancer Res. Treat.* **42**(2) (1997), 165–172.

[45] V. Vukovic, T. Nicklee and D.W. Hedley, Multiparameter fluorescence mapping of nonprotein sulfhydryl status in relation to blood vessels and hypoxia in cervical carcinoma xenografts, *Int. J. Radiat. Oncol. Biol. Phys.* **52**(3) (2002), 837–843.

[46] N. Weidner, J.P. Semple, W.R. Welch and J. Folkman, Tumor angiogenesis and metastasis – correlation in invasive breast carcinoma, *N. Engl. J. Med.* **324**(1) (1991), 1–8.

[47] K. Wester, P. Ranefall, E. Bengtsson, C. Busch and P.U. Malmstrom, Automatic quantification of microvessel density in urinary bladder carcinoma, *Br. J. Cancer* **81**(8) (1999), 1363–1370.

[48] K.I. Wijffels, J.H. Kaanders, P.F. Rijken, J. Bussink, F.J. van den Hoogen, H.A. Marres, P.C. de Wilde, J.A. Raleigh and A.J. van der Kogel, Vascular architecture and hypoxic profiles in human head and neck squamous cell carcinomas, *Br. J. Cancer* **83**(5) (2000), 674–683.

[49] R. Wild, S. Ramakrishnan, J. Sedgewick and A.W. Griffioen, Quantitative assessment of angiogenesis and tumor vessel architecture by computer-assisted digital image analysis: effects of VEGF-toxin conjugate on tumor microvessel density, *Microvasc. Res.* **59**(3) (2000), 368–376.

[50] T. Williams, Image understanding tools, *Proc. ICPR10* **2** (1990), 606–610.